Electronic Supporting information (ESI)

Electronic Modulation at an Ag/La(OH)$_3$ Crystalline-Amorphous Heterostructure Enables High-Efficiency CO_2-to-CO Conversion

Ziyin Xie, Na Wu, Leili Wang, Lihui Dong, Danyang Li, Bin Li, Zhengjun Chen*

Green Chemical New Materials Engineering Research Center of Guangxi Colleges and Universities, Guangxi Key Laboratory of Electrochemical Energy Materials, School of Chemistry and Chemical Engineering, Guangxi University, Nanning, 530004, China.

**E-mail address: zjchen@gxu.edu.cn (Z. Chen)*

Experimental section

Material

Sodium borohydride ($NaBH_4$, AR) and potassium bicarbonate ($KHCO_3$, AR) were purchased from Tianjin Kermel Chemical Reagent Co., Ltd. Silver nitrate ($AgNO_3$, 98%) was purchased from Guangdong Guanghua Sci-Tech Co., Ltd. Potassium hydroxide (KOH, AR) and sodium hydroxide (NaOH, AR) were purchased from Chengdu Kelong Chemical Co., Ltd. Lanthanum nitrate hexahydrate ($La(NO_3)_3 \cdot 6H_2O$, 99.0%), dihydrate zinc acetate ($Zn(CH_3COO)_2$, 99.9%) and Nafion perfluoro alkoxy resin (5% in a mixture of lower aliphatic alcohols and water, containing 45% water) were purchased from Shanghai Macklin Biochemical Co., Ltd. N, N-dimethylformamide (DMF, AR) was purchased from Tianjin Fuyu Fine Chemical Co., Ltd. Hydrophobic carbon paper was purchased from Toray Industries, Inc. Nafion 117 proton exchange membrane was purchased from DuPont. All chemicals were used directly without any purification

Material

Synthesis of Ag/La(OH)$_3$ catalysts. Briefly, a series of Ag/La(OH)$_3$ catalysts with different La(OH)$_3$ contents were prepared by co-dissolving $AgNO_3$ and $La(NO_3)_3 \cdot 6H_2O$ in 10 mL of DMF. The feeding Ag/La atomic ratios were controlled at 100/1, 50/1, and 30/1, and the corresponding samples are denoted as Ag/La(OH)$_3$-1, Ag/La(OH)$_3$-2, and Ag/La(OH)$_3$-3, respectively. Thereafter, 5 mL of deionized water was introduced, and stirred for an additional 0.5 h. The resulting product was collected by centrifugation, washed thoroughly with deionized water and ethanol, and dried under vacuum at 60 °C for 12 h. For comparison, the Ag sample and pristine La(OH)$_3$ were synthesized using the identical procedure without the addition of $La(NO_3)_3 \cdot 6H_2O$ and Ag precursor, respectively. The Ag/La atomic ratio in the Ag/La(OH)$_3$ sample was determined to be 45:1 through quantitative analysis via inductively coupled plasma optical emission spectrometry (ICP-OES).

Characterization

Inductively coupled plasma (ICP) analysis was conducted using an Agilent 720ES optical emission spectrometer (OES). X-ray diffraction (XRD) patterns were collected

on a Rigaku D/MAX-2500/PC diffractometer with Cu K_α radiation (λ = 1.5418 Å) at 40 kV and 20 mA. Data were acquired at room temperature over a 2θ range of 10-90° with a scanning rate of 10° min^{-1}. The infrared spectra were measured using a Nicolet iS50 Fourier transform infrared spectrometer. Transmission electron microscopy (TEM) was performed on a JEM-2100 microscope operating at 200 kV. High-resolution TEM (HRTEM) images and energy-dispersive X-ray spectroscopy (EDS) mapping were acquired using a JEM-ARM200F microscope at 200 kV. X-ray photoelectron spectroscopy (XPS) measurements were carried out on a Thermo Scientific K-Alpha spectrometer with an Al K_α X-ray source. The obtained spectra were processed using Avantage software, with all binding energies calibrated against the C 1s peak at 284.0 eV.

Electrochemical Measurements

10 mg of catalyst was dispersed in a mixed solvent consisting of 350 μL ethanol, 600 μL deionized water, and 50 μL Nafion solution (5 wt%), and sonicated for 1 hour to obtain a homogeneous dispersion. 100 μL of this dispersion was drop-cast onto a 1×1 cm^2 carbon paper, with the catalyst loading controlled at 1 mg cm^{-2}, and dried at room temperature for subsequent use.

Electrochemical testing was conducted using a three-electrode system with a CHI 660E electrochemical workstation (Shanghai Chenhua Instrument Co., Ltd.). The working electrode was the carbon paper loaded with catalyst (1 × 1 cm^2), the reference electrode was an Ag/AgCl electrode, and the counter electrode was a Pt plate electrode. Prior to testing, the cathode compartment electrolyte (0.5 M $KHCO_3$) was pre-saturated with high-purity CO_2 (99.99%) for 30 minutes. During testing, a mass flow controller (D07-19B, Shenzhen Xinlisheng Technology) was used to maintain a CO_2 flow rate of 20 sccm. A Nafion-117 proton exchange membrane was used as the separator, an H-type cell was employed, with each electrode chamber containing 40 mL of 0.5 M $KHCO_3$ electrolyte. The scan rate for both cyclic voltammetry (CV) and linear sweep voltammetry (LSV) tests was 10 mV s^{-1}. All potential data were converted to reversible hydrogen electrode (RHE) scale according to the following equation:

$$E \text{ (vs. RHE)} = E \text{ (vs. Ag/AgCl)} + 0.197 + 0.0591 \times \text{pH}$$

A 90% iR compensation was applied to all potentials according to the formula below:

E(corrected)=E(measured)-iR, where R is the uncompensated solution resistance.

Electrochemical active surface area (ECSA) was quantified by measuring the double-layer capacitance (C_{dl}). Specifically, cyclic voltammetry (CV) tests were conducted in a CO_2-saturated 0.5 M $KHCO_3$ electrolyte within the non-Faradaic reaction potential window. By establishing a linear relationship between geometric current density and scan rate at different scan rates, the C_{dl} value was calculated using the slope of the linear regression. Electrochemical impedance spectroscopy (EIS) tests were performed in a CO_2-saturated environment, with the frequency range set from 10^5 Hz to 10^{-2} Hz. Gas product analysis was performed using an online gas chromatography system (FULI, GC-9790II) equipped with a flame ionization detector (FID) and a thermal conductivity detector (TCD) combination device. The Faraday efficiency (FE) of each reduction product was calculated using the following equation:

$$FE\ (\%) = (n \times N \times F) / Q_{total} \times 100\%$$

In the equation: n represents the molar quantity of the product (mol); N represents the number of electrons transferred in the CO_2 reduction reaction (in this study, N = 2); F represents the Faraday constant (96485 C mol^{-1}); Q_{total} represents the cumulative total electric charge of the electrolysis process (C).

Electrochemical Measurements

A bipolar membrane (BPM) was used to separate the H-type electrochemical cell into independent anode and cathode chambers, thereby establishing an aqueous Zn-CO_2 electrolysis system. The anode electrolyte consists of a 1 M $KHCO_3$ solution saturated with CO_2, while the cathode electrolyte was a mixture of 0.02 M $Zn(CH_3COO)_2$ and 1 M KOH. The anode used polished zinc foil, while the cathode consisted of catalyst-coated carbon paper. During electrochemical testing, the CO_2 flow rate was precisely controlled using a mass flow meter (20 sccm).

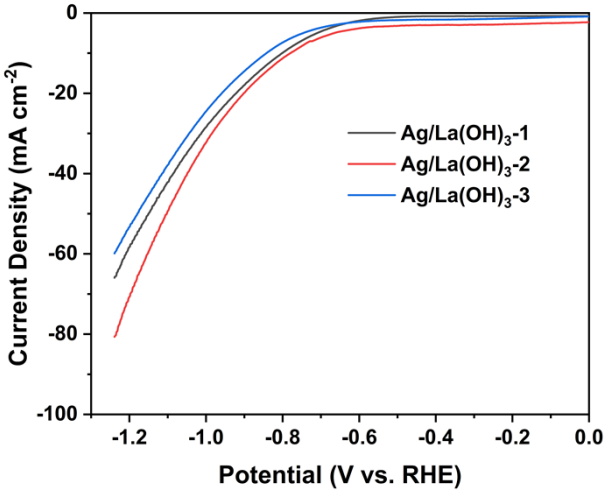

Fig. S1 LSV curves of Ag/La(OH)$_3$ catalyst at different Ag/La feeding atomic ratio.

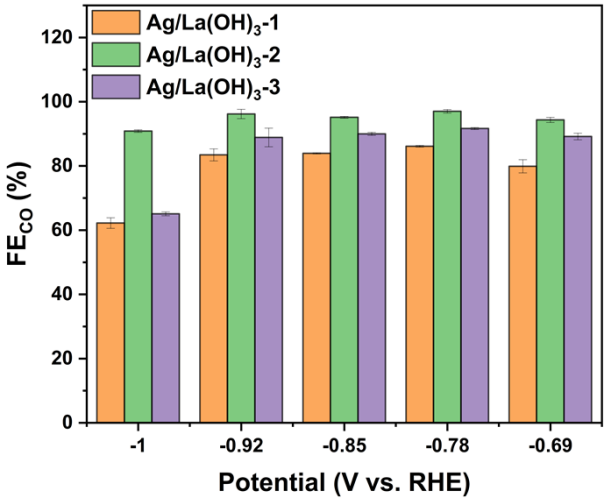

Fig. S2 FE$_{CO}$ of Ag/La(OH)$_3$ catalyst at different Ag/La feeding atomic ratio.

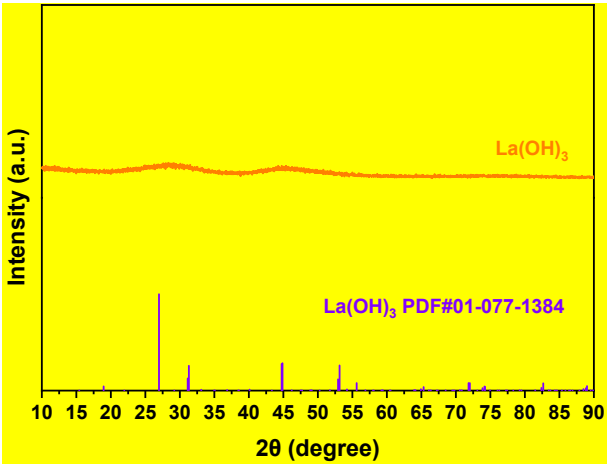

Fig. S3 XRD pattern of La(OH)$_3$

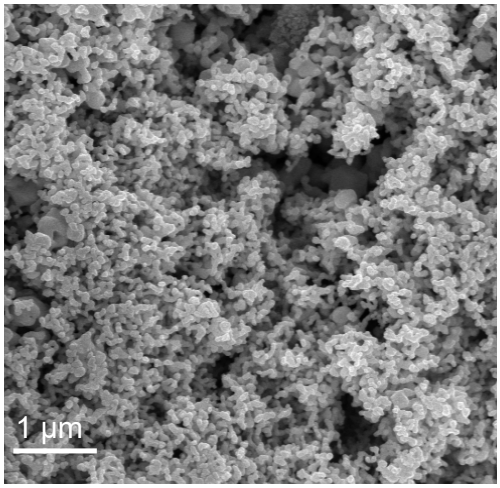

Fig. S4 SEM image of Ag catalyst.

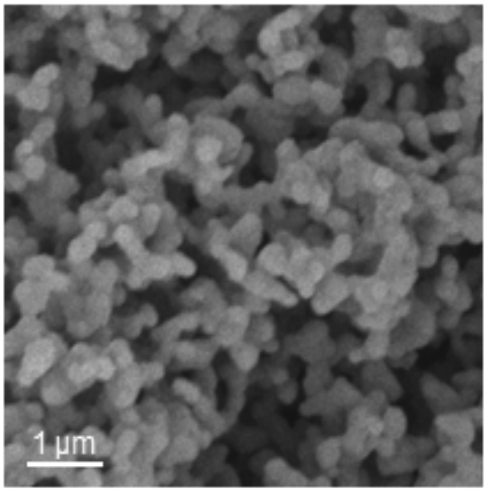

Fig. S5 SEM image of Ag/La(OH)$_3$ catalyst after stability testing.

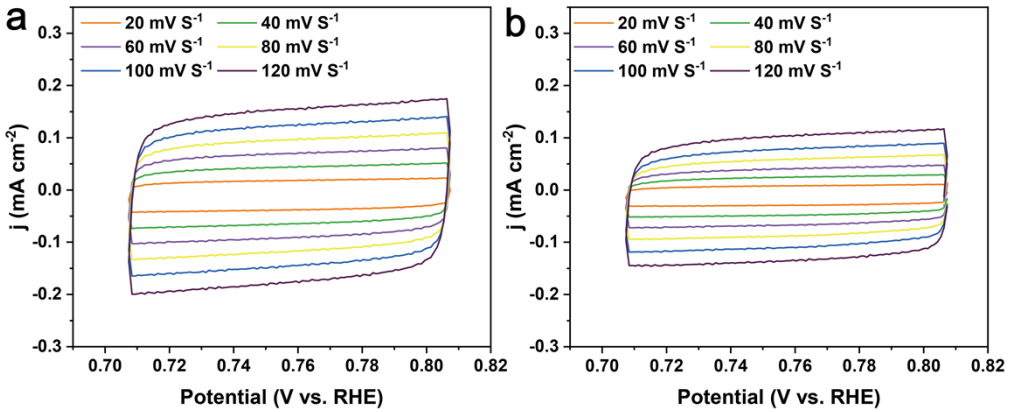

Fig. S6 Electrochemical double-layer capacitance measurements of (a) Ag/La(OH)$_3$ catalyst and (b) Ag catalyst.

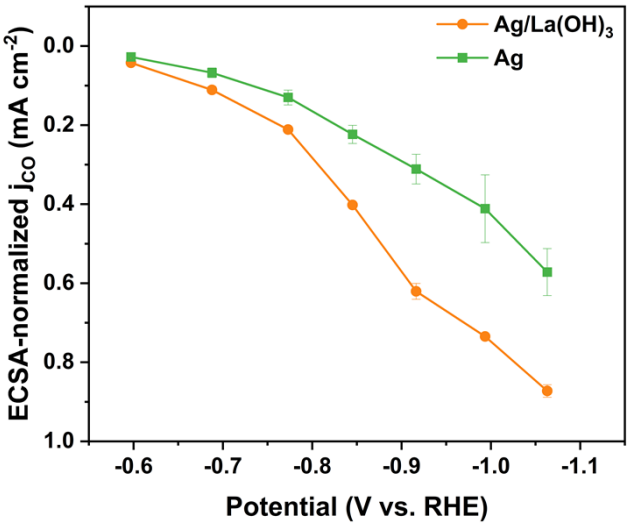

Fig. S7 ECSA normalized j_{CO} for $Ag/La(OH)_3$ catalyst and Ag catalyst.

Table S1. Electrochemical performance of different Ag-based catalysts for CO production.

Electrocatalysts	Potential vs. RHE	Electrolytes	FE_{CO} (%)	Ref.
$Ag/La(OH)_3$	**-0.78 V**	**0.5 M $KHCO_3$**	**97.6**	**This work**
CV-actived Ag	-0.7 V	0.5 M $KHCO_3$	96.6	[1]
Ag/h-Cu_2O	-0.96 V	0.1 M $KHCO_3$	93	[2]
Ag-$In(OH)_3$/C	-0.7 V	0.1 M $KHCO_3$	93	[3]
ZnO-Ag@UC	-0.93 V	0.5 M $KHCO_3$	94.1	[4]
Ag-MnO_x	-0.8 V	0.5 M $KHCO_3$	97.5	[5]
Ag/Ov-CeO_2	-0.9 V	0.1 M $KHCO_3$	96.3	[6]
AgCu NP	-0.5 V	1 M KOH	85	[7]
Ag-BTC	-1.0 V	0.1 M $KHCO_3$	95	[8]
Cu/Ag(S)	-1.0 V	0.1 M $KHCO_3$	93	[9]

1 Y. Mao, Q. Mao, H. Yang, Q. Liu, X. Dong, Y. Li, S. Zhou and B. Liu, *Angew. Chem., Int. Ed.*, 2024, **63**, e202410932.
2 J. Li, Z. Cheng, J. Zhu, H. Chen, X. Xu, Y. Wang, J. Liu, Z. Xu and L. Wang, *Appl. Catal., B*, 2024, **352**, 124049.
3 L. Fu, Z. Qu, L. Zhou and Y. Ding, *Appl. Catal., B*, 2023, **339**, 123170.
4 Z. Zhang, G. Wen, D. Luo, B. Ren, Y. Zhu, R. Gao, H. Dou, G. Sun, M. Feng, Z. Bai, A. Yu and Z. Chen, *J. Am. Chem. Soc.*, 2021, **143**, 6855-6864.
5 C. Wen, Z. Xie, N. Wu, L. Dong, B. Li and Z. Chen, Interfacial interaction of Ag-MnO_x heterostructure for efficient CO_2 electroreduction to CO and aqueous Zn-CO_2 batteries. *Inorganic Chemistry Frontiers*, 2025, 12, 4324-4333.
6 Y. F. Tang, S. Liu, M. Yu, P.-F. Sui, X. Z. Fu, J. L. Luo and S. Liu, *ACS Appl. Mater. Interfaces*, 2024, **16**, 41669-41676.
7 M. Śliwa, H. Zhang, J. Gao, B. O. Stephens, A. J. Patera, D. Raciti, P. D. Hanrahan, Z. A. Warecki, D. L. Foley, K. J. T. Livi, T. H. Brintlinger, M. L. Taheri, A. S. Hall and T. J. Kempa, *Nano Lett.*, 2024, **24**, 13911-13918.
8 W. Yu, S. Chen, J. Zhu, Z. He and S. Song, *J. CO2 Util.*, 2023, **70**, 102457.
9 Z. Ma, T. Wan, D. Zhang, J. A. Yuwono, C. Tsounis, J. Jiang, Y.-H. Chou, X. Lu, P. V. Kumar, Y. H. Ng, D. Chu, C. Y. Toe, Z. Han and R. Amal, *ACS Nano*, 2023, **17**, 2387-2398.